Progress In Electromagnetics Research C, Vol. 115, 161–174, 2021

Dual Band Circularly Polarized Modified Ψ-Shape Microstrip Antenna

Amit A. Deshmukh* **and Anuja A. Odhekar**

Abstract—Single patch designs of a microstrip antenna with a U-slot or a pair of rectangular slots (E-shape) provide a single band circularly polarized response, and hence they are not useful in frequency and polarization agile applications. In this paper, a modified design of a Ψ-shape microstrip antenna is proposed for dual band and dual sense circularly polarized response. Use of unequal length rectangular slots in the modified patch optimizes the inter-spacing between the modified TM_{21} and TM_{22} resonant modes, surface current distributions and impedance levels at them to yield dual band circularly polarized response. An impedance bandwidth of 1992 MHz (37.05%) is obtained which completely covers the axial ratio bandwidth of 11.84 and 5.67%, in the two bands with a frequency ratio of 1.3 in between them, thereby satisfying the requirements of frequency agile systems. Over the impedance and axial ratio bandwidth, the antenna exhibits nearly broadside radiation pattern with a gain of around 7 dBi. A design methodology based on the simple parametric formulation is presented, which helps in realizing a similar antenna in the specific frequency band. The proposed antenna can find applications in frequency and polarization agile systems where the signal loss due to the interference and jamming can be reduced.

1. INTRODUCTION

Due to the numerous advantages, microstrip antenna (MSA) finds maximum usage in the modern day wireless communication applications [1, 2]. In wireless applications, because of the multi-path propagation effect, received signal undergoes changes in its polarization and thus lead to a signal loss [3]. To minimize it, circularly polarized (CP) antennas are selected [3]. By using a single radiating patch, the MSA can generate a CP response which proves to be its major advantage, while looking at the total system cost [1, 2]. In MSA, CP response is realized by introducing dual orthogonal modes which satisfies the phase orthogonality condition [3]. In the initial designs, by feeding the MSA using dual feeds, the CP response has been realized [4, 5]. Later, using a single coaxial feed, narrow slot cut designs of square MSA, circular MSA, and equilateral triangular MSA are reported to obtain the CP response [5–10]. Most of these single and dual feed MSAs were optimized on thinner substrates, and hence they offer lower axial ratio (AR) bandwidth (BW). On a thinner substrate, high gain wide band CP designs using shorting pins are reported [11–14]. The shorting pins are used in reducing the antenna size, and hence they offer a smaller gain [1, 2, 5]. Therefore, which of the shorted patch modes that yields high gain and wide band CP characteristics is not clearly explained in [11–14]. By suitably modifying the regular shape geometry on an air suspended substrate, narrow to wideband CP designs have been realized [15–17]. By using parasitic patches and power divider circuit, a wide band CP response, offering AR BW in the range of 8 to 10%, is reported [18, 19]. By embedding a U-slot or a pair of rectangular slots (E-shape), CP designs offering 5–7% of AR BW is reported [20–22, 41]. Although these designs are suspended single patch configuration, they offer single band CP response. Hence, they are not suitable in frequency agile applications. A wideband design of a Ψ-shape MSA is reported in [23]. By modifying

Received 28 June 2021, Accepted 1 September 2021, Scheduled 13 September 2021
* Corresponding author: Amit A. Deshmukh (amitdeshmukh76@gmail.com).
The authors are with the EXTC Department, DJSCE, Mumbai, India.

the geometry of a regular Ψ-shape MSA, its wideband CP design is reported [24]. However, the reported configuration is complicated in design and does not provide any explanation to highlight the effects of modifications incorporated in the original patch in realizing wideband CP characteristics. By embedding fractal U-shape slots on the ground plane, a narrow band CP response (AR BW $\sim 1\%$) is reported [25]. In the frequency and polarization agile systems, the antenna operating in two CP bands is needed. The dual band and dual sense CP response is realized by using different techniques like use of circular patch fed using the power divider circuit that operates around the fundamental and higher order patch modes [26]. Dual-band CP MSAs are also realized by using modified patch shapes backed by the slot cut ground plane [27, 28], or the use of slot cut patches [29–31] and shorted and slot cut patches [32], which are operating near the fundamental and modified higher order mode frequencies. Using an assembly of stacked patches fed using either coaxial or aperture feed [33, 34], or the gap-coupled configuration of multiple patches fed using the proximity feed on electrically thicker substrate [35, 36], dual-band CP response has been realized. Here the use of power divider increases the design complexities, whereas in the modified patch shape and slot cut and shorted patch designs, detailed explanation for the antenna working in terms of orthogonal modes present and subsequent design methodology is not discussed. Further, the use of multiple patches in the same or stacked layer increases the antenna size. Thus, a simpler single layer and single patch design is needed which can offer dual band CP response.

In this paper, initially a wideband design of a Ψ-shape MSA is discussed on a suspended FR4 substrate ($\varepsilon_r = 4.3$, $h = 0.16\,\text{cm}$). Further for the same antenna dimensions, an unequal slot length design of modified Ψ-shape MSA is proposed. To explain the effects of unequal slot lengths, a detailed parametric study for the variations in slot length that forms the equivalent E-shape and Ψ-shape MSA is presented. It is shown that unequal slot length optimizes the inter-spacing between the TM_{21} and TM_{22} resonant modes of the modified Ψ-shape MSA, which yields dual band CP response. In the two bands, AR BWs of 561 MHz (11.84%) and 347 MHz (5.67%) are obtained, which lie inside the impedance BW of 1992 MHz (37.05%). The proposed antenna yields CP response with a smaller frequency ratio of 1.3, in between the two bands. In addition, in the first CP band, the proposed antenna yields right hand CP (RHCP) response whereas in the second band, it yields left hand CP (LHCP) response. Across the impedance and AR BW, antenna yields the gain around 7 dBi with a nearly broadside radiation pattern. Thus compared with the reported dual band CP designs, the proposed design is a single patch configuration offering more than 5% AR BW in each band with smaller frequency ratio in between them and with a gain around 7 dBi. Against the slot cut CP variations, the proposed design yields dual band CP response that will be useful in frequency agile systems. A detailed comparison highlighting the novelty against the reported configurations is presented further in the paper. Based on the optimum CP configuration, design methodology using simple parametric formulation is presented. The Ψ-shape MSA designed using them in different frequency bands yields similar dual band CP response. The proposed dual band design can find applications in frequency and polarization agile systems, where a signal loss occurring because of the multi-path propagation, interference, and jamming can be minimized. The dual band Ψ-shape MSA is initially studied using CST software [45]. For analyzing the antenna response, finite rectangular ground plane of dimension $13 \times 8.5\,\text{cm}$ with SMA panel type connector feed is used. Experimental validation for the obtained results is carried out using high frequency instruments namely, ZVH-8, FSC 6, and SMB 100A.

2. ANALYSIS OF MODIFIED Ψ-SHAPE MSA FOR DUAL BAND CP RESPONSE

The modified design of Ψ-shape MSA is shown in Figs. 1(a), (b). The units for the patch dimensions and frequency referred throughout the paper are in 'cm' and 'MHz', respectively. Initially in the wideband variation of Ψ-shape MSA, antenna dimensions are selected to be the same as that reported in [23]. However, the patch is fabricated on a low cost FR4 substrate, and it is suspended above the ground plane using an air gap of 'h_a' = 0.5 cm, thereby realizing total antenna height ($h_t = h_a + h$) nearly the same as that given in [23]. For 'L_s' = 'L_{s1}' = 1.9, 'L_{s2}' = 2.3 and 'w_s' = 0.6 cm, wideband Ψ-shape MSA yields simulated impedance BW of 2753 MHz (56.66%). For the MSAs reported in [20, 21, 41], by embedding unequal length slots, bi-directional variation in surface currents is realized over the slot cut patch that gives single band CP response. In wideband Ψ-shape MSA, modified TM_{21} mode exits towards the higher frequencies of the BW that leads to bi-directional current variation over the

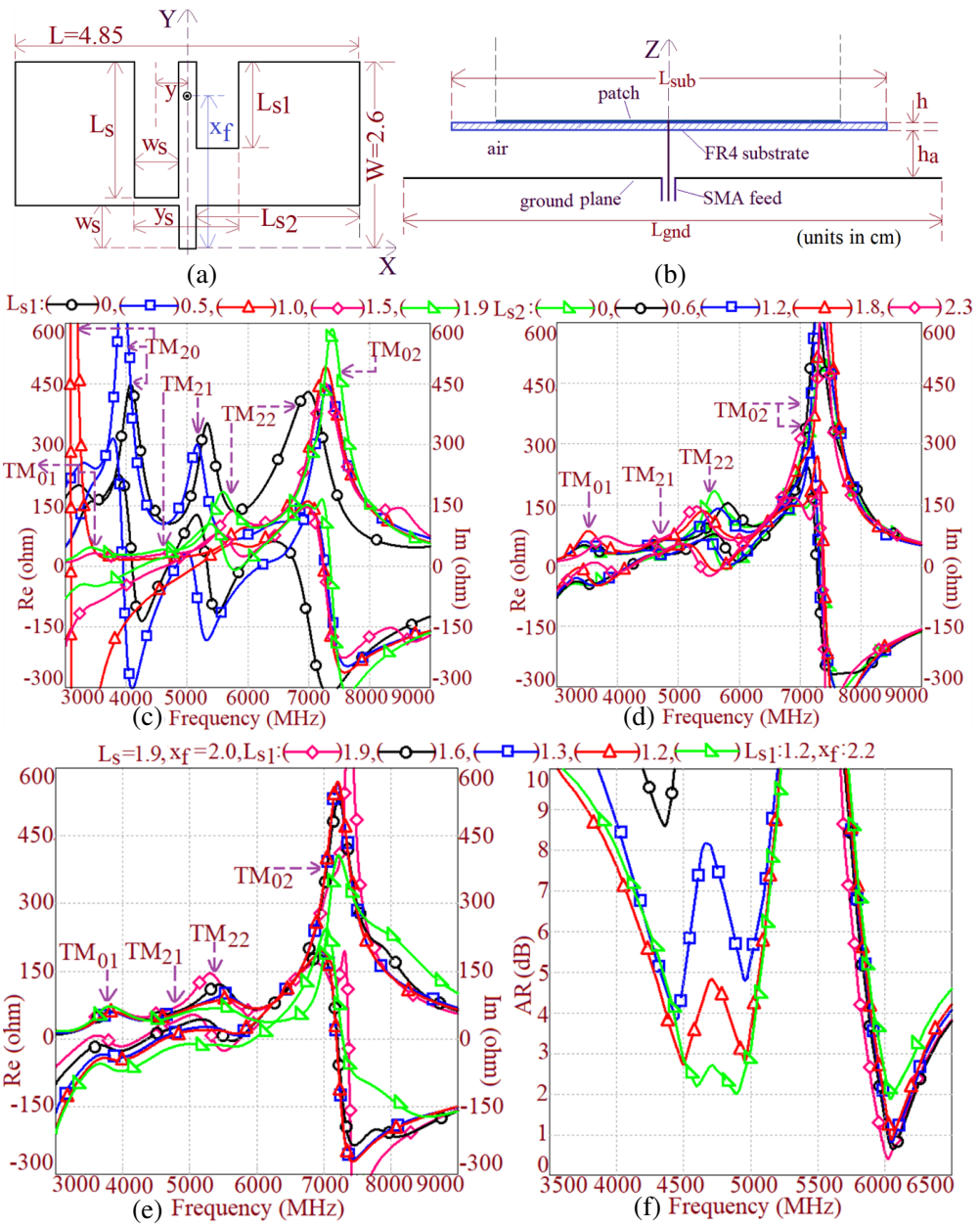

Figure 1. (a) Top and (b) side views of modified Ψ-shape MSA, resonance curve plots for variation in (c) L_{s1} (L_s), (d) L_{s2}, (e) resonance curve and (f) axial ratio plots for variation in unequal slot length 'L_{s1}'.

patch [46]. However as equal slot lengths are present in wideband Ψ-shape MSA, bi-directional current contribution is smaller. Hence an unequal slot length design of Ψ-shape MSA is explored, hereto strengthens the bi-directional current variation for the CP response, as shown in Figs. 1(a), (b).

Since the Ψ-shape MSA is a modified variation of an E-shape MSA, a detailed analysis is presented here to explain the effects of slot lengths 'L_s', 'L_{s1}', and 'L_{s2}' on the realized wideband and CP response. Initially lengths 'L_s' and 'L_{s1}', which form the E-shape structure are cut followed by the length 'L_{s2}', which is cut along the non-radiating edge of the equivalent RMSA that realizes Ψ-shape geometry. Further, the effects of selecting unequal lengths 'L_s' and 'L_{s1}' are studied. The resonance curve plots and surface current distributions at the observed resonant modes for these length variations are shown in Figs. 1(c)–(f) and Figs. 2(a)–(i).

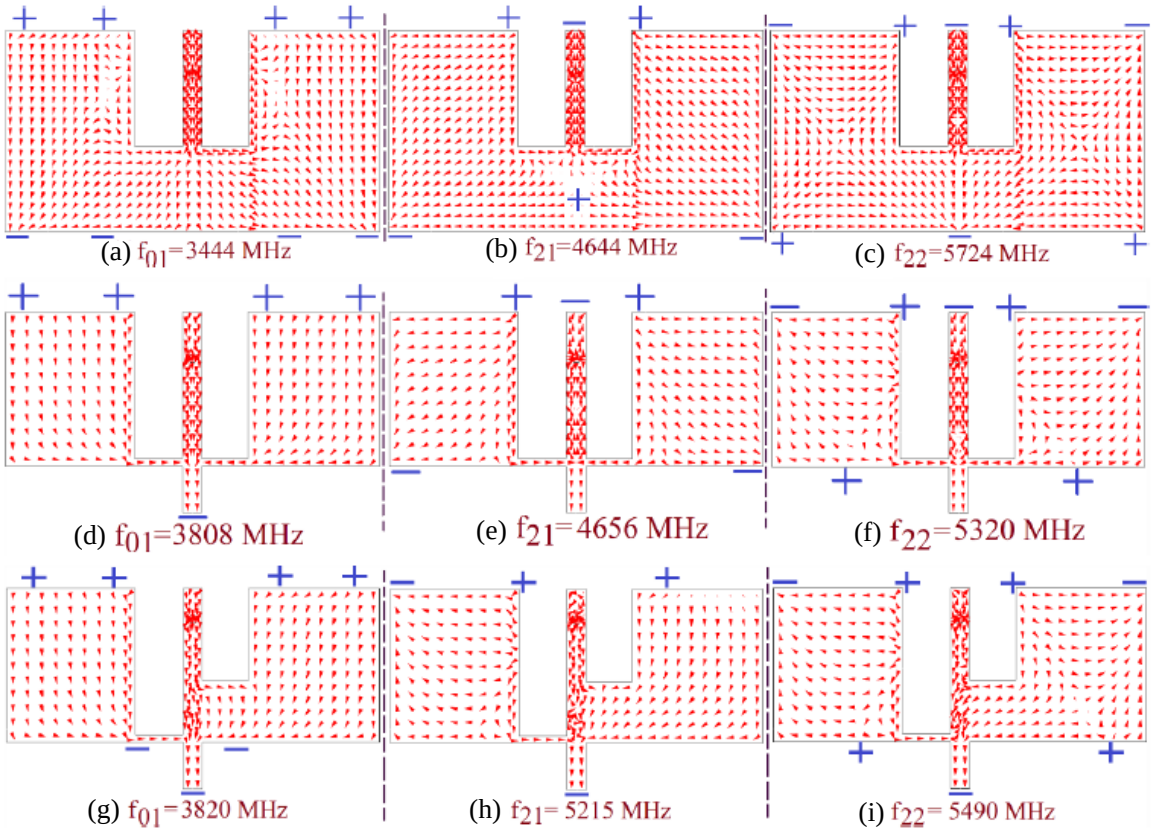

Figure 2. Surface current distributions at the observed resonant modes for (a)–(c) E-shape MSA, 'L_s' = 'L_{s1}' = 1.5 cm, (d)–(f) Ψ-shape MSA, 'L_{s2}' = 2.3 cm and (g)–(i) modified Ψ-shape MSA, 'L_s' = 1.9 and 'L_{s1}' = 1.2 cm.

The vector surface current plots are given against the average one, as the direction of modal currents is needed to be analysed for the CP generation. The fringing field distribution for the respective modes is in correlation with the modal current distributions as observed on the patch. To differentiate in each of the plots showing parametric variations, respective curves are shown using different colours and markers. The length of the equivalent RMSA is almost twice the width, which gives smaller W/L ratio (0.54). At the feed location for TM_{01} mode excitation, TM_{20} mode also gets excited. This leads to a close spacing between the frequencies of TM_{01} and TM_{20} modes in the resonance curve. A smaller 'W/L' ratio also yields close spacing of other orthogonal higher order modes with respect to the fundamental mode. The resonant mode identification for the RMSA and slots cut RMSA is carried out by studying the vector surface current distributions at each resonant peak as well as by studying the variations in their frequencies against the slot length increments. While realizing E-shape MSA first, lengths 'L_s' and 'L_{s1}' are increased together. With an increase in 'L_{s1}' (L_s), the frequency of TM_{20} mode reduces as the surface currents at the TM_{20} mode are orthogonal to the increasing slot length. For the length more than 1.0 cm, TM_{20} mode frequency decreases below the TM_{01} mode frequency. The frequencies of TM_{21} and TM_{22} modes also decrease with an increase in slot length 'L_s' (L_{s1}). For 'L_s' = 1.5 cm, surface currents at TM_{01} mode exhibit variations along the modified patch width and length. The variation along the patch length is due to the close proximity of TM_{20} mode, whose frequency is below the TM_{01} mode frequency. At modified TM_{21} and TM_{22} modes, the surface currents show bi-directional variation over the patch with the field polarities as shown. At positive field polarity, fringing fields originate from the patch and terminate on the ground whereas at the negative field polarity, they originate from the ground and terminate on the patch. With an increase in slot length 'L_{s2}', which realizes the Ψ-shape structure, the TM_{01} mode frequency increases. This increment is attributed to the reduction in the patch width as seen by the modal currents. The TM_{21} mode frequency marginally varies whereas the

TM_{22} mode frequency decreases with an increase in 'L_{s2}'. With the variation in 'L_{s2}', surface current variation remains bi-directional over the Ψ-shape patch. The CP response in slot cut MSA is realized either due to the close proximity of dual orthogonal modes or due to the bi-directional variation in the surface currents on the slot cut patch around the given mode frequencies [1, 2, 21]. Thus, bi-directional current variation as observed over the Ψ-shape MSA gives the possibility of realizing CP response. To strengthen this bi-directional current variation over modified TM_{21} and TM_{22} modes, unequal slot lengths in E-shape design are considered, and their effects on the modal frequencies and AR BW are studied, as shown in Figs. 1(e), (f). In this length variation, for 'L_s' = 1.9 and 'L_{s2}' = 2.3 cm, length 'L_{s1}' is decreased. Against the decrease in 'L_{s1}', TM_{01} mode frequency remains unchanged, whereas TM_{21} and TM_{22} mode frequencies slightly increase. Further, the impedance level at TM_{22} mode reduces. The surface current distributions at TM_{21} and TM_{22} modes remain bi-directional over the modified Ψ-shape MSA, but their contributions are strengthened such that the AR value reduces to below 3 dB.

3. RESULTS AND DISCUSSIONS

As seen from the above analysis, unequal slot lengths strengthen the bi-directional surface current variation over the patch in TM_{21} and TM_{22} modes and optimize the impedance level and frequency separation between them that gives dual band CP response for AR less than 3 dB, as shown in Figs. 1(f) and 3(a), (b). The antenna parameters in the optimum CP design are 'L_s' = 1.9, 'L_{s1}' = 1.2, 'L_{s2}' = 2.3, 'x_f' = 2.2 cm. The antenna shows simulated and measured BWs for reflection coefficient (S_{11}) less than −10 dB of 1992 MHz (37.05%) and 2000 MHz (37.66%), respectively. The simulated AR BWs for AR less than 3 dB in the two CP bands are 561 MHz (11.84%) and 347 MHz (5.67%), respectively. The measured values of the AR BW are 550 MHz (11.74%) and 374 MHz (6.16%). Over the impedance and AR BW, antenna gain is around 7 dBi. Since higher order TM_{21} and TM_{22} resonant modes are responsible for realizing the CP response, the gain maximum and AR BW are observed in the direction $\Phi = 0°$, $\theta = 15°$. This change of the maximum gain and AR BW direction simply requires reorientation of the antenna plane along the θ-axis, against the orientation of the antenna in Φ and θ planes, as required for the design reported in [24].

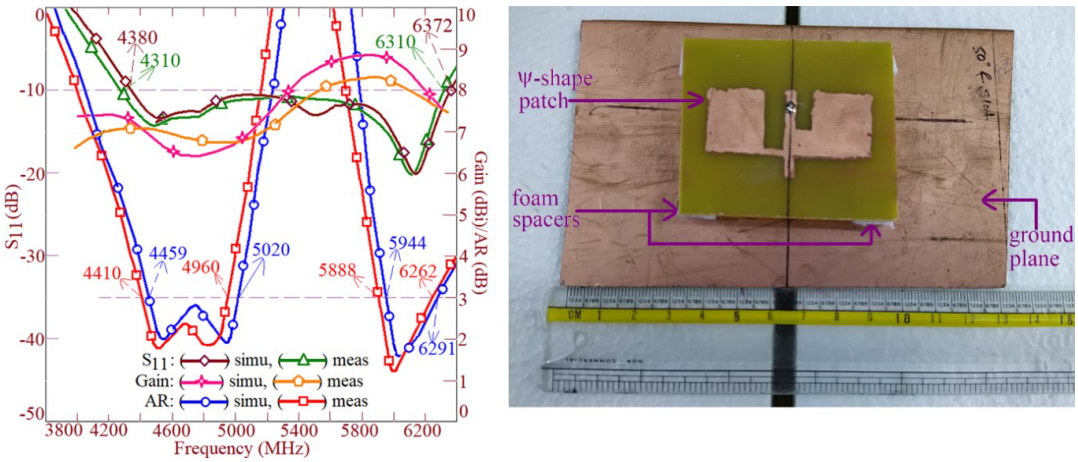

Figure 3. (a) S_{11}, gain and AR BW plots and (b) fabricated prototype for dual band modified Ψ-shape MSA.

Thus, the proposed antenna is simpler in orientation to the reported design of modified Ψ-shape MSA. Due to thicker substrate, the AR beamwidths in the two CP bands are around 30° to 35°. The radiation patterns at the center frequency and across the complete AR BW in two CP bands show nearly broadside radiation with co and cross polarization levels within 3 dB difference, as shown in Figs. 4(a)–(d).

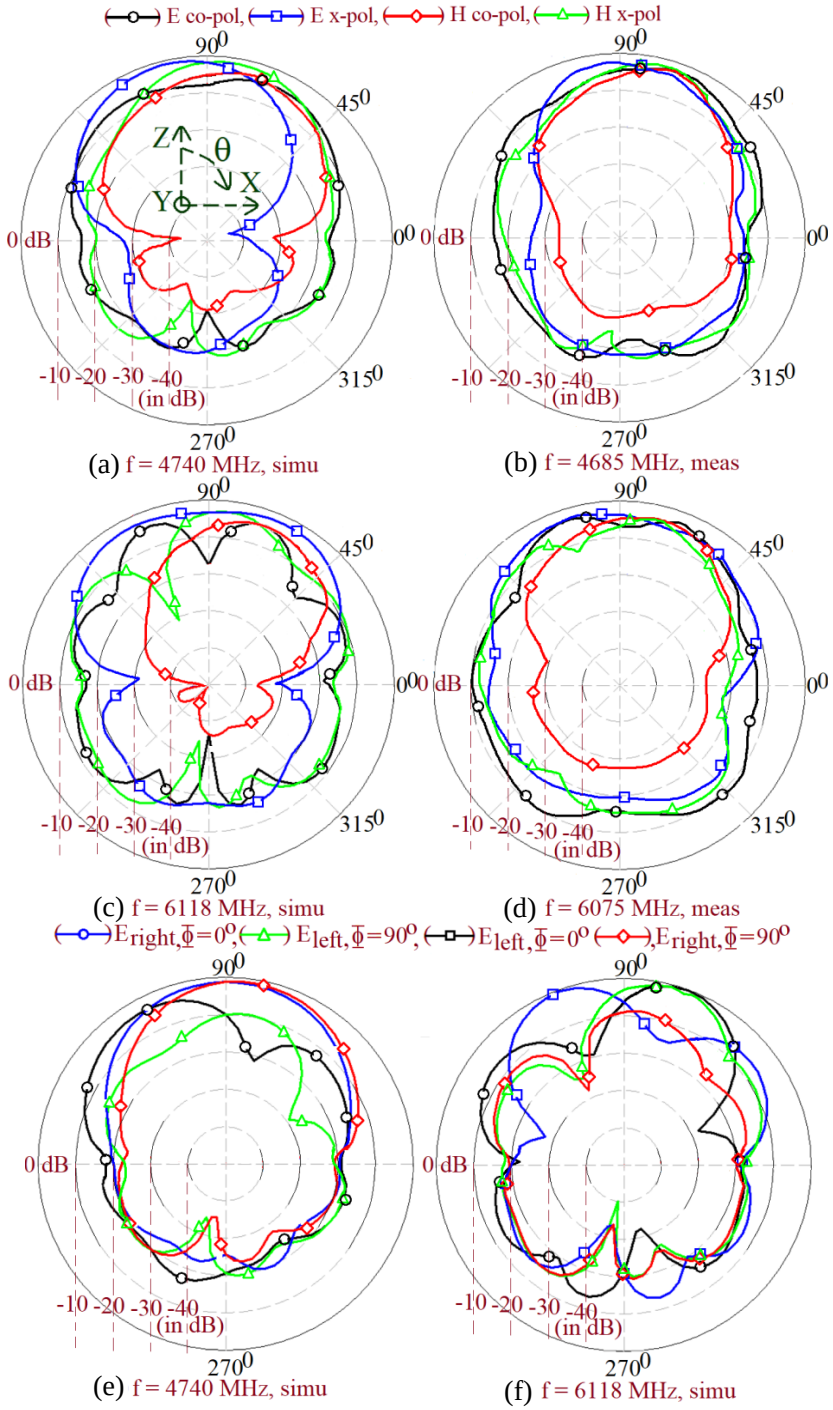

Figure 4. (a)–(d) Radiation patterns at the center frequency of the two CP bands, respectively, (e), (f) simulated polarization plots, for dual band modified Ψ-shape MSA.

To analyze the sense of rotation, i.e., RHCP or LHCP response, simulated polarization plots and time varying surface current distribution at the center frequency of the AR BW are studied as shown in Figs. 4(e), (f) and Figs. 5(a)–(h). Along $\theta = 15°$, in the lower band, right hand CP waves are dominant whereas in the higher band, left hand CP waves are dominant with a difference of 10 dB with respect to their left or right hand counterparts.

In the first CP band, with reference to one side of the modified patch, surface currents rotate in the

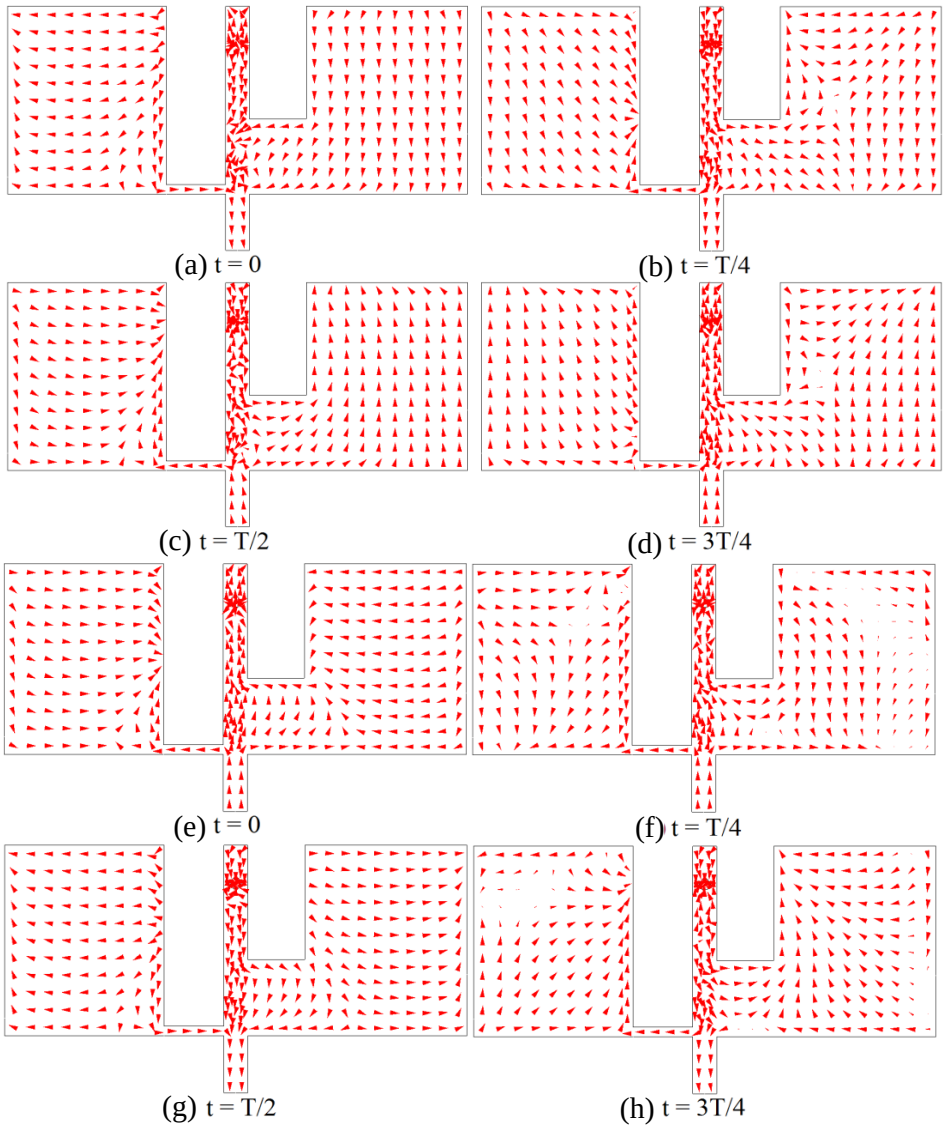

Figure 5. Time varying surface current distribution in (a)–(d) first and (e)–(h) second CP band for dual band dual sense modified Ψ-shape MSA.

clockwise direction, thereby giving RHCP response. In the second band, on the same patch side, sense of rotation is reversed which gives LHCP response. As the polarity of field/current component reverses on the other patch side, the sense of rotation is observed to be opposite there. Further sense of CP rotation was verified experimentally. Here, a nearly square MSA reference antenna was used as transmitter in each band. For the LHCP and RHCP feed excitation, when the sense of rotation of the transmitter antenna is matched with the receiver, received power is maximum. For the other rotation, received power reduces by more than 8–10 dB. Thus the above simulated and experimental results confirm the CP response for a given sense of rotation in the two bands. The setup for the measurement of various antenna parameters is shown in Figs. 6(a), (b). In the radiation pattern and gain measurement, which is carried out inside the Antenna Lab, reference wideband horn antennas were used. The broadside gain is measured using the three antenna method. The far field distance between reference antenna and antenna under test is calculated with respect to the wavelength in higher CP band. With reference to the lower CP band frequency, the distance of the surrounding objects is more than eight times the wavelength that ensures minimum reflections. Thus in comparison with the reported U-slot and pair of

Figure 6. (a) Pattern, gain and (b) impedance measurement setup for the dual band modified Ψ-shape MSA.

rectangular slots cut CP MSAs, the proposed unequal slot length Ψ-shape MSA yields dual band dual sense CP response, thereby making it useful in frequency and polarization agile systems.

4. PARAMETRIC DESIGN FORMULATION FOR MODIFIED Ψ-SHAPE MSA

In the above dual band configuration, simulated band start frequency (f_{startAR}) of the first CP band is 4459 MHz, whereas the TM_{01} mode frequency (f_{01}) of the equivalent RMSA is 3430 MHz. This gives frequency ratio of 1.3 in between them. Using this frequency relation, a redesign procedure is presented for the specific band start frequency of the first CP band. Thus, for the given band start frequency, TM_{01} mode frequency of the RMSA is calculated by using Equation (1). The dual band MSA is designed on a suspended FR4 substrate. For the suspended dielectric substrate, initial value of the effective dielectric constant (ε_{re}) is unknown, since it depends upon the air gap present between the suspended substrate and the ground plane. Hence, an initial assumption of 'ε_{re}' as 1.2 is chosen. This value is selected based upon the value of effective dielectric constant as calculated for the suspended dielectric in the above optimum dual band design. Using this value, TM_{01} mode operating wavelength (λ_g) and total substrate thickness (h_t) are calculated using Equations (2) and (3), respectively. In terms of the wavelength, the value of 'h_t' has been selected to be the same as that present in the above optimum dual band design. This total substrate thickness equals the air gap 'h_a' plus the substrate thickness of the FR4 layer 'h'. For this calculated value of 'h_t', practically realizable value of 'h_a' is selected. Using this value of 'h_a', effective dielectric constant value is recalculated using Equation (4). In this equation 'ε_r' equals the dielectric constant of FR4 substrate. Using this value of 'ε_{re}', 'h_t' and subsequently practically realizable value of 'h_a' are decided. This iterative procedure is carried out once, since the initial value of 'ε_{re}' is unknown. The values of 'h_a' and 'ε_{re}', as calculated in the first assumption case and that calculated after the first iterative process, differ by a small margin. For further calculation, a new value of 'ε_{re}' as calculated using Equation (4) is used. The RMSA length 'L' and width 'W' are calculated using Equations (5) and (6), respectively.

$$f_{01} = {f_{\text{startAR}}}/{1.3} \tag{1}$$

$$\lambda_g = {30}/{f_{01}\sqrt{\varepsilon_{re}}} \tag{2}$$

$$h_t = 0.092\lambda_g \tag{3}$$

$$\varepsilon_{re} = {1.2\varepsilon_r\,(h + h_a)}/{\varepsilon_r h_a + h} \tag{4}$$

$$W = \left({30}/{2f_{01}\sqrt{\varepsilon_{re}}}\right) - 1.4\,(h_a + h) \tag{5}$$

$$L = 1.865W \tag{6}$$

Based upon the optimum values of various antenna parameters as present in the original dual band design, parametric formulation for them is realized. The slot dimensions 'L_s', 'L_{s1}', 'L_{s2}', and 'w_s' are

selected to be $0.266\lambda_g$, $0.168\lambda_g$, $0.322\lambda_g$, and $0.085\lambda_g$, respectively. The separation between the two slots (y) which forms the equivalent E-shape geometry is taken to be $0.0595\lambda_g$, whereas the coaxial feed point is placed at 'x_f' = 0.846 W. The dual band antenna is designed using this procedure for f_{startAR} of nearly 3500 MHz, i.e., for $f_{\text{TM01}} = 2700$ MHz. Using the above procedure, in some of the antenna parameters, practically not realizable values are obtained which are further rounded off to the practically realizable values. Hence, in some of the antenna parameters, marginal parametric optimization is needed further to get the optimum response. Various antenna parameters for this optimum redesigned antenna are, $h_a = 0.7$, $L = 6.5$, $W = 3.5$, $L_s = 2.5$, $L_{s1} = 1.6$, $L_{s2} = 3.0$, $w_s = 0.8$, $y = 0.55$, $x_f = 2.95$ cm. The S_{11}, gain, AR BW plots, and the fabricated antenna prototype are shown in Figs. 7(a), (b). The antenna fabricated on an FR4 layer is suspended above the ground plane using foam spacers ($\varepsilon_r \sim 1.06$) which are placed towards the corners of the patch. The SMA panel type connector is used to feed the antennas. The redesigned modified Ψ-shape MSA shows the simulated and measured S_{11} BWs of 1422 MHz (34.07%) and 1404 MHz (34.23%), respectively. The simulated AR BWs in the two CP bands are 436 MHz (11.73%) and 218 MHz (4.6%), respectively. The measured values of the AR BW are 437 MHz (11.8%) and 233 MHz (5.0%). Over the impedance and AR BW, average antenna gain is around 7 dBi.

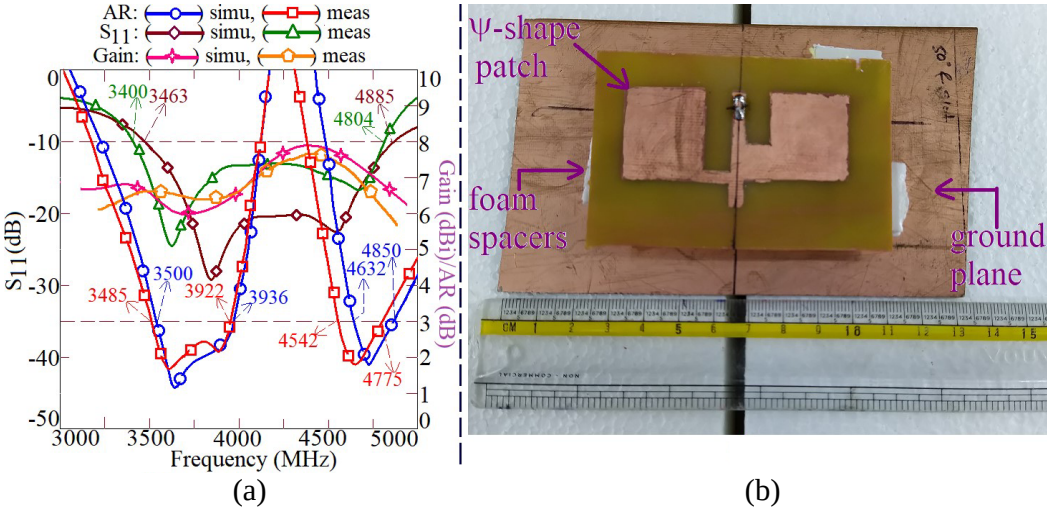

Figure 7. (a) S_{11}, gain and AR BW plots, and (b) fabricated prototype for dual band modified Ψ-shape MSA re-designed for $f_{\text{startAR}} = 3500$ MHz, ($f_{\text{TM01}} = 2700$ MHz).

Thus using the proposed redesigning procedure, start frequency of the first CP band matches with the required frequency of 3500 MHz. Using the above procedure, antenna was also designed for $f_{\text{startAR}} = 4200$ MHz. In this design also, simulated and measured frequency of the start frequency of the first CP band is around 4230 MHz, thereby matching closely with the required value. Thus the proposed design methodology is useful in the design of CP antenna around the given frequency band on thicker suspended substrate.

To highlight the novelty, the comparison of the proposed design against the reported CP variations is presented in Table 1. The patch area (A_p) and total substrate thickness (h_t), as mentioned in Table 1, is normalized with respect to the wavelength (λ_c) at the center frequency of the first CP band. The respective values of the impedance and AR BW and the patch dimensions are noted from the respective reported papers. The comparison is presented against the single and dual band CP variations. The multi-band antennas are useful in frequency agile application, which helps in reducing the signal loss due to the interference. For the given CP design, if the AR BW obtained is sufficiently large, then agility is realized within the same CP band. Hence for the comparison purpose single band and dual band CP designs are considered. The low profile designs as presented in [7, 8] offering single band CP response have smaller AR BW and lower gain. Using shorted single patch, higher gain single band CP response is obtained [11–14]. However, which of the shorted patch modes that contribute to this CP response is

Table 1. Comparison of the modified Ψ-shape MSA against reported CP designs.

Reported MSA, Ref no.	Meas BW (MHz, %)	Meas AR BW (MHz, %)	A_p/λ_c	Peak Gain (dBi)	h_t/λ_c
[7]	—	band 1: 10, 0.6	2.1	—	0.014
[8]	—	band 1: 14, 0.87	1.215	—	0.018
[11]	110, 4.3	band 1: 34, 1.33	1.912	10.3	0.04
[15]	705, 43.7	band 1: 170, 10.7	1.873	7.5	0.129
[16]	3.5, 2.2	band 1: 8, 0.5	10.87	3.9	0.023
[17]	653, 54	band 1: 79, 6.4	> 2.3	8.5	0.108
[18]	305, 30.95	band 1: 81, 8.95	7.022	7.0	0.11
[19]	450, 27	band 1: 260, 16	5.3	8.0	0.158
[20]	255, 15.2	band 1: 50, 3.2	1.045	4.5	0.153
[22]	810, 35	band 1: 130, 5.3	2.362	9	0.101
[24]	2000, 40	band 1: 1000, 19	3.542	7.5	0.12
[25]	30, 1.9	band 1: 6, 0.4	1.358	2.3	0.052
[26]	—	band 1: 22, 2.386 band 2: 170, 6.84	1.267	band 1: 3.8 band 2: 8.9	0.027
[27]	band 1: 1210, 38.8 band 2: 1540, 27.5	band 1: 1150, 37.4 band 2: 890, 16.3	7.652	band 1: 4.3 band 2: 3.3	0.034
[28]	band 1: 500, 20.41 band 2: 630, 12.56	band 1: 400, 16.6 (RHCP) band 2: 300, 5.72 (LHCP)	1.343	band 1: 1.9 band 2: 1.3	0.02
[29]	band 1: 15, 0.6 band 2: 15, 0.5	band 1: 20, 0.826 band 2: 25, 0.862	0.653	band 1: 1.3 band 2: 2.9	0.02
[30] Ant. I	band 1: 400, 25 band 2: 270, 10.8	band 1: 90, 5.6 (LHCP) band 2: 50, 2 (RHCP)	4.46	band 1: 3.6 band 2: 3.9	0.01
[31]	—	band 1: 148, 5.92 (RHCP) band 2: 160, 2.46 (LHCP)	—	band 1: 3.8 band 2: 5.5	0.014
[32]	band 1: 130, 5.3 band 2: 470, 13.6	band 1: 70, 2.84 band 2: 55, 1.57	3.993	band 1: -0.1 band 2: 4.2	0.072
[33]	band 1: 355, 16.19 band 2: 315, 11.28	band 1: 46, 2.1 band 2: 50, 2.0	1.443	band 1: 7.0 band 2: 8.3	0.064
[34]	band 1: 29, 2.99 band 2: 24, 2.72	band 1: 9, 1.07 (RHCP) band 2: 11, 1.19 (LHCP)	2.973	band 1 & 2: > 4.5	0.114
[35]	band 1: 38, 1.8 band 2: 94, 2.6	band 1: 9, 0.4 band 2: 21, 0.6	1.246	band 1: 8.4 band 2: 9.9	0.036
[37]	500, 35.71	band 1: 120, 9.6 band 2: 110, 7.1	3.765	band 1: 1.98 band 2: 4.1	0.032
Fig. 1(a)	**2000, 37.66**	**band 1: 550, 11.74, (RHCP) band 2: 374, 6.16, (LHCP)**	**2.245**	**band 1: 7.0 band 2: 8.3**	**0.118**

not explained in detail. Further, the realized AR BW on relatively thicker substrate (~ 0.03–$0.04\lambda_c$) is smaller. The single band antenna using modified patch shapes as reported in [15] although offers higher AR BW and gain, here the design methodology is not presented. For the modified patch design as reported in [17], detailed design methodology is presented, but the reported antenna requires larger patch size due to the overlap patches. Further, designs using parasitic co-planar patches [18, 19] offer higher AR BW but have larger patch size. In addition, those designs employ power divider that adds

to the overall design requirements. The U-slot and rectangular slot cut designs as reported in [20–22] offer smaller AR BW in a single band, whereas the design reported in [24] is complex in design and in the orientation, as the CP response is obtained in different 'θ' and 'Φ' angles. The fractal design employed in [25] is complex in implementation and has AR BW less than 1%. The dual band CP design as reported in [26] requires power divider for exciting the orthogonal modes closer to the fundamental and higher order resonant modes of the circular patch whereas for the design reported in [27], a detailed explanation for the orthogonal modes that yields this dual band higher AR BW CP response is not discussed. In addition, the patch size is larger, and the gain is lower. The dual band design reported in [28] does offer dual sense CP response with switching of diodes, but realized gain is lower in both the bands. In addition, the details about the functioning of antenna in terms of modes present in the modified patch and subsequent design methodology are not explained. As compared with the proposed design, the antennas reported in [29–31] have lower impedance, AR BW, and the gain. The dual band CP design as reported in [32] employs slots on the patch and ground plane along with the shorting post, which makes their implementation complex, whereas in the proposed design, only slots are used. Further, the shorted MSA reported in [32] has lower AR BW and gain in the two bands. The designs reported in [33–35] require two patches catering to the two CP bands and offer lower AR BW. They have comparable values of the patch area and substrate thickness as compared with the proposed modified Ψ-shape MSA. Although the design reported in [37] offers higher values of the AR BW in the two bands, it employs multiple stacked circular patches along with a power divider circuit. Due to this the reported design has larger patch area and lower gain as well. Using diagonal slots on thinner substrate circular or rectangular patches, CP design offering higher AR beam width is reported [38–40]. However, those designs offer single band CP response with lower AR BW and thus cannot find applications in frequency and polarization agile systems. Using a reconfigurable E-shape patch, a single band CP design with 8% AR BW is reported [41]. The compact design of Sectoral MSA using a shorting plate and slot is reported in [42]. Against these, the proposed design is dual bands, simpler due to the absence of any shorting as well as offers much higher gain than the shorted sectoral patch. Using a coupled ring resonator or metamaterial structure, CP antennas are reported [43, 44]. Against these, the proposed design is simpler single patch design, offers dual band CP response and thus satisfies the requirements of frequency and polarization agile systems.

Against all the reported dual band CP configurations, the proposed design is a single patch design. It is simpler in implementation since it uses only unequal length slots. The proposed antenna offers higher gain and AR BW in the two bands with dual sense polarization across them. Due to the higher order modes present, CP response is obtained along $\theta = 15^\circ$. Since the angular adjustment is needed only in one direction, antenna orientation is very simple against the design, which requires antenna orientation for the CP waves in 'θ' and 'Φ' directions. Against the unequal length U-slot and rectangular slots cut design, the proposed antenna yields dual band dual sense CP response thereby making it useful in frequency and polarization agile systems. The design guidelines are presented based upon the parametric optimization, which are helpful in the designing of the proposed configuration around the specific band start frequency of the first CP band. Thus, a novel simpler single patch design of modified Ψ-shape MSA offering dual band dual sense CP response with appreciably higher values of the gain and AR BW makes new technical contributions in the proposed work. The proposed antenna can find applications in frequency and polarization agile systems.

5. CONCLUSIONS

The design of a modified Ψ-shape MSA for dual band CP response is presented. An unequal slot length in the Ψ-shape patch yields an optimum separation between the modified TM_{21} and TM_{22} resonant modes along with the optimization of the impedance levels at them that yields dual frequency CP response. The measured AR BWs of 550 MHz (11.74%) and 374 MHz (6.16%) in two bands which is residing inside the impedance BW of 2000 MHz (37.66%) is obtained. The antenna offers dual sense CP response across the two bands with peak gains around 7 and 8.3 dBi, in the two bands. Thus, a simpler single patch slots cut design offering dual band dual sense CP response is the new technical contribution in the present work against the reported designs.

REFERENCES

1. Garg, R., P. Bhartia, I. Bahl, and A. Ittipiboon, *Microstrip Antenna Design Handbook*, Artech House, Norwood, USA, 2001.
2. Bahl, I. J. and P. Bhartia, *Microstrip Antennas*, Artech House, USA, 1980.
3. Balanis, C. A., *Antenna Theory: Analysis and Design*, 2nd Edition, John Wiley & Sons Ltd., USA, 1996.
4. Deshpande, M. D. and N. K. Das, "Rectangular microstrip antenna for circular polarization," *IEEE Trans. Antennas Propag.*, Vol. 34, No. 6, 744–746, 1986.
5. Kumar, G. and K. P. Ray, *Broadband Microstrip Antennas*, 1st Edition, Artech House, USA, 2003.
6. Wong, K. L., *Compact and Broadband Microstrip Antennas*, 1st Edition, John Wiley & Sons, New York, USA, 2002.
7. Suzuki, Y., N. Mitano, and T. Chiba, "Circularly polarized radiation from singly fed Equilateral-triangular microstrip antenna," *IEE Proceedings H*, Vol. 134, No. 2, 194–198, 1987.
8. Lu, J.-H., H.-C. Yu, and K.-L. Wong, "Compact circular polarization design for equilateral-triangular microstrip antenna with spur lines," *Electronic Letters*, Vol. 34, No. 21, 1989–1990, 1998.
9. Lu, J.-H. and K.-L. Wong, "Single-feed circularly polarized equilateral-triangular microstrip antenna with a tuning stub," *IEEE Trans. Antennas Propag.*, Vol. 48, No. 12, 1869–1872, 2000.
10. Nageswara Rao, P. and N. V. S. N. Sarma, "Koch fractal boundary single feed circularly polarized microstrip antenna," *Journal of Microwaves, Optoelectronics and Electromagnetic Applications*, Vol. 6, No. 2, 406–413, 2007.
11. Zhang, X. and L. Zhu, "High-gain circularly polarized microstrip patch antenna with loading of shorting pins," *IEEE Trans. Antennas Propag.*, Vol. 64, No. 6, 2172–2178, 2016.
12. Tran, H. H., N. Nguyen-Trong, and H. C. Park, "A compact wideband omnidirectional circularly polarized antenna using TM_{01} mode with capacitive feeding," *IEEE Antennas and Wireless Propagation Letters*, Vol. 18, No. 1, 19–23, 2019.
13. Shi, Y. and J. Liu, "Wideband and Low profile omni-directional circularly polarized antenna with slits and shorting vias," *IEEE Antennas and Wireless Propagation Letters*, Vol. 15, 686–689, 2016.
14. Zhang, X., L. Zhu, and N. Liu, "Pin-loaded circularly-polarized patch antennas with wide 3-dB axial ratio bandwidth," *IEEE Trans. Antennas Propag.*, Vol. 65, No. 2, 521–528, 2017.
15. Deng, J.-Y., L.-X. Guo, T.-Q. Fan, Z.-S. Wu, Y.-J. Hu, and J. H. Yang, "Wideband circularly polarized suspended patch antenna with indented edge and gap-coupled feed," *Progress In Electromagnetics Research*, Vol. 135, 151–159, 2013.
16. Shi, Y. and J. Liu, "A circularly polarized octagon-star-shaped microstrip patch antenna with conical radiation pattern," *IEEE Trans. Antennas Propag.*, Vol. 66, No. 4, 2073–2078, 2018.
17. Deshmukh, A. A. and K. P. Ray, "Circularly polarized designs of modified isosceles triangular microstrip antennas," *Engineering Reports*, Wiley Publication, https://onlinelibrary.wiley.com/doi/10.1002/eng2.12250.
18. Sim, C. Y. D., C. C. Chen, R. Cao, and B. S. Chen, "A circular patch antenna with parasitic element for UHF RFID applications," *International Journal of RF Microwave and Computer Aided Engineering*, Vol. 25, No. 8, 681–687, 2015.
19. Fu, S., Q. Kong, S. Fang, and Z. Wang, "Broadband circularly polarized microstrip antenna with coplanar parasitic ring slot patch for L-band satellite system application," *IEEE Antennas and Wireless Propagation Letters*, Vol. 13, 943–946, 2014.
20. Lam, K. Y., K.-M. Luk, K. F. Lee, H. Wong, and K. B. Ng, "Small circularly polarized U-slot wideband patch antenna," *IEEE Antennas and Wireless Propagation Letters*, Vol. 10, 87–90, 2011.
21. Khidre, A., K. F. Lee, F. Yang, and A. Elsherbeni, "Wideband circularly polarized E-shaped patch antenna for wireless applications," *IEEE Antennas & Propagation Magazine*, Vol. 52, No. 5, 219–229, 2010.

22. Kovitz, J. M., H. Rajagopalan, and Y. Rahmat-Samii, "Circularly polarised half E-shaped patch antenna: A compact and fabrication-friendly design," *IET Microwave Antennas and Propagation*, Vol. 10, No. 9, 932–938, 2016.
23. Sharma, S. K. and L. Shafai, "Performance of a novel Ψ-shaped microstrip patch antenna with wide bandwidth," *IEEE Antennas and Wireless Propagation Letters*, Vol. 8, 468–471, 2009.
24. Mondal, T., S. Maity, R. Ghatak, and R. B. S. Chaudhuri, "Design and analysis of a wideband circularly polarized perturbed Psi-shaped antenna," *IET Microwaves, Antennas & Propagation*, Vol. 12, No. 9, 1582–1586, 2018.
25. Wei, K., J. Y. Li, L. Wang, R. Xu, and Z. J. Xing, "A new technique to design circularly polarized microstrip antenna by fractal defected ground structure," *IEEE Trans. Antennas Propag.*, Vol. 65, No. 7, 3721–3725, 2017.
26. Liu, Q., J. Shen, J. Yin, H. Liu, and Y. Liu, "Compact 0.92/2.45 GHz dual-band directional circularly polarized microstrip antenna for handheld rfid reader applications," *IEEE Trans. Antennas Propag.*, Vol. 63, No. 9, 3849–3856, 2015.
27. Rui, X., J. Li, and K. Wei, "Dual-band dual-sense circularly polarized square slot antenna with simple structure," *Electronics Letters*, Vol. 52, No. 8, 578–580, 2016.
28. Kumar, P., S. Dwari, R. K. Saini, and M. K. Mandal, "Dual band dual sense polarization reconfigurable circularly polarized antenna," *IEEE Antennas and Wireless Propagation Letters*, Vol. 18, No. 1, 64–68, 2019.
29. Samsuzzaman, Md. and M. T. Islam, "Dual frequency circularly polarized cross-shaped slotted patch antenna with a small frequency ratio," *Microwave and Optical Technology Letters*, Vol. 56, No. 11, 2711–2719, 2014.
30. Lei, Z.-Y., J. Zhang, R. Yang, X. Liu, L. Chen, and X. Kong, "Design of dual-band dual-sense circularly polarized slot antenna," *Progress In Electromagnetics Research C*, Vol. 43, 41–51, 2013.
31. Shao, Y. and Z. Chen, "A design of dual-frequency dual-sense circularly-polarized slot antenna," *IEEE Trans. Antennas Propag.*, Vol. 60, No. 11, 4992–4997, 2021.
32. Zhang, H.-Y., F.-S. Zhang, C. Wang, and T. Li, "Dual-band omnidirectional circularly polarized patch antenna with etched slots and shorting vias," *Progress In Electromagnetic Research C*, Vol. 73, 167–176, 2017.
33. Deng, C. J., Y. Li, Z. Zhang, G. Pan, and Z. Feng, "Dual-band circularly polarized rotated patch antenna with a parasitic circular patch loading," *IEEE Antennas and Wireless Propagation Letters*, Vol. 12, 492–495, 2013.
34. Wang, Z., R. She, J. Han, S. Fang, and Y. Liu, "Dual-band dual-sense circularly polarized stacked patch antenna with a small frequency ratio for UHF RFID reader applications," *IEEE Access*, Vol. 5, 15260–15270, 2017.
35. Liang, Z.-X., D.-C. Yang, X.-C. Wei, and E.-P. Li, "Dual-band dual circularly polarized microstrip antenna with two eccentric rings and an arc-shaped conducting strip," *IEEE Antennas and Wireless Propagation Letters*, Vol. 15, 834–837, 2016.
36. Deshmukh, A. A., A. Doshi, and A. Odhekar, "Gap coupled design star shape microstrip antenna for dual band and wide band circular polarized response," *International Journal of RF and Microwave, Computer Aided Engineering*, Vol. 29, No. 5, 664–674, 2019.
37. Liu, H., C. Xun, S.-J. Fang, and Z. Wang, "Compact dual-band circularly polarized patch antenna with wide 3-dB axial ratio beamwidth for BeiDou applications," *Progress In Electromagnetic Research M*, Vol. 87, 103–113, 2019.
38. Ray, M. K., K. Mandal, N. Nasimuddin, A. Lalbaksha, R. Raad, and F. Tubbal, "Two-pair slots inserted CP patch antenna for wide axial ratio beamwidth," *IEEE Access*, Vol. 8, 223316–223324, 2020.
39. Ray, M. K. and K. Mandal, "Pair of diagonal slots loaded low-profile circularly polarised patch antenna with wide 3 dB axial ratio beamwidth," *IET Microwave Antennas and Propagation*, Vol. 13, No. 14, 2433–2438, 2019.

40. Ray, M. K., K. Mandal, and N. Nasimuddin, "Low profile circularly polarized patch antenna with wide 3-dB beamwidth," *IEEE Antennas and Wireless Propagation Letters*, Vol. 18, No. 12, 2473–2477, 2019.
41. Khidre, A., K. Lee, F. Yang, and A. Z. Elsherbeni, "Circular polarization reconfigurable wideband E-shaped patch antenna for wireless applications," *IEEE Trans. Antennas Propag.*, Vol. 61, No. 2, 960–964, 2013.
42. Yu, J., W.-J. Lu, Y. Cheng, and L. Zhu, "Tilted circularly polarized beam microstrip antenna with miniaturized circular sector patch under wideband dual-mode resonance," *IEEE Trans. Antennas Propag.*, Vol. 68, No. 9, 6580–6590, 2020.
43. Ameen, M. and R. K. Chaudhary, "A compact circularly polarized antenna using CRLH inspired transmission line and coupled ring resonator," *AEU International Journal of Electronics and Communication*, 2020, https://doi.org/10.1016/j.aeue.2020.153238.
44. Khandelwal, M. K., "Metamaterial based circularly polarized four-port MIMO diversity antenna embedded with slow-wave structure for miniaturization and suppression of mutual coupling," *AEU International Journal of Electronics and Communication*, 2020, https://doi.org/10.1016/j.aeue.2020.153241.
45. CST Microwave studio, Version 2019.
46. Deshmukh, A. A. and K. P. Ray, "Analysis of broadband Ψ-shaped microstrip antennas," *IEEE Antennas and Propagation Magazine*, Vol. 55, No. 2, 107–123, 2013.